ELSEVIER

Journal of Hazardous Materials A88 (2001) 1–32

Journal of Hazardous Materials

www.elsevier.com/locate/jhazmat

Modelling of catastrophic flashing releases

D.M. Deaves*, S. Gilham, B.H. Mitchell, P. Woodburn, A.M. Shepherd

WS Atkins Consultants Ltd., Woodcote Grove, Ashley Road, Epsom, Surrey KT18 5BW, UK

Received 15 April 2000; received in revised form 29 May 2001; accepted 1 June 2001

Abstract

Several low boiling point materials are stored in closed vessels at ambient temperature, using their own vapour pressure to maintain a liquid state. These materials are often toxic, flammable, or both, and thus any uncontrolled release can have potentially disastrous consequences. There are many ways in which an accidental release can occur, the most severe being due to catastrophic vessel failure. Although not the most common, this mode of failure has the potential to result in an instantaneous loss of the entire vessel inventory in the form of a rapidly expanding, two-phase, vaporising cloud. This paper provides a comprehensive review of the physical processes of existing models and of available experimental and incident data to model such scenarios. Subsequently, this has enabled the development of an improved methodology for the characterisation of the source conditions following catastrophic vessel failures.

Keywords: Flashing releases; Catastrophic failures; CFD modelling; Source term model

1. Introduction

Toxic and flammable materials are frequently stored under pressure, such that vessel failure would result in energetic catastrophic flashing releases. In a review of a number of such catastrophic incidents, Slater [1] demonstrated that, for this type of event, the effects are consistently felt over a large area, frequently resulting in loss of life or causing extensive damage. An example of such an incident occurred on 13 July 1973, at a South African fertiliser plant [2], when one of four 50 t horizontal cylindrical ammonia pressure storage vessels failed. The failure was caused by a brittle fracture of the dished end and resulted in the release of an estimated 38 t of anhydrous ammonia. The release immediately produced a gas cloud 150 m in diameter and 20 m in depth which slowly dispersed in a light wind;

* Corresponding author.
E-mail address: dmdeaves@wsatkins.co.uk (D.M. Deaves).

0304-3894/01/$ – see front matter
PII: S0304-3894(01)00284-9

Nomenclature

b	dimensionless constant in k–ε model
C	fitted constant in cloud volume equation
$C_{2\varepsilon}$	dimensionless constant in k–ε model
D_d	Sauter mean droplet diameter (m)
E_0	total specific energy in state 0 (J/kg)
E_1	total specific energy in state 1 (J/kg)
E_a	work done in expanding the cloud (J/kg)
h_fg	heat of vaporisation (J/kg)
k	turbulent energy density ($\mathrm{m^2/s^2}$)
k_d	thermal conductivity of droplet (W/m/K)
KE_1	kinetic energy of state 1 per unit mass (J/kg)
$\dot{m}_\mathrm{d}$	material flashing rate (kg/s)
M	initial stored mass of material (kg)
P_a	ambient pressure ($\mathrm{N/m^2}$)
ΔP	pressure difference across orifice ($\mathrm{N/m^2}$)
$\dot{q}$	heat flow through the droplet (J/s)
r	characteristic radius of the cloud (m)
r_d	droplet radius (m)
s_g1	entropy of gaseous phase in state 1 (J/kg)
$s_{\lambda 0}$	entropy of liquid phase in state 0 (J/kg)
$s_{\lambda 1}$	entropy of liquid phase in state 1 (J/kg)
t	time (s)
ΔT	temperature difference between droplet and environment (K)
u	air velocity (m/s)
u_d	droplet velocity (m/s)
u_L	turbulent velocity (m/s)
U_1	specific internal energy (J/kg)
V_c	cloud volume ($\mathrm{m^3}$)
We	Weber number
X	flash fraction

Greek letters

ε	energy dissipation due to viscosity (J/kg/s)
ν_d	droplet viscosity ($\mathrm{N/m^2/s}$)
ρ_1	density in state 1 ($\mathrm{kg/m^3}$)
ρ_0	density in state 0 ($\mathrm{kg/m^3}$)
ρ_a	ambient density ($\mathrm{kg/m^3}$)
ρ_d	droplet density ($\mathrm{kg/m^3}$)
ρ_sva	saturation vapour density at the storage temperature ($\mathrm{kg/m^3}$)
ρ_va	vapour density at ambient temperature and pressure ($\mathrm{kg/m^3}$)
σ_d	droplet surface tension (N/m)

the visible cloud reached 300 m in diameter and moved approximately 450 m downwind of the release point. Toxic effects of the ammonia caused the deaths of 18 people.

Given the potential toxic or flammable nature of the materials stored as pressure liquefied gases, quantified risk assessments (QRA) requiring some form of consequence analysis are frequently undertaken for installations which contain such materials.

For a large instantaneous release resulting from the catastrophic failure of the containment vessel, the spreading of the material starts with an initial rapid expansion, as described by Schmidli et al. [3]. This expansion is principally driven by the stored internal energy, and is assumed to end when the cloud turbulence has decayed to atmospheric levels. This initial stage is arguably the most important, but least understood, probably explaining why so few models describing it exist.

In order to improve the predictions of such events, various studies were undertaken, for which full details have been presented by Gilham et al. [4]. These studies include the following factors.

- Identified release characteristics and defined a phenomenological model.
- Considered the impact of catastrophic releases on risk.
- Reviewed current models and available data.
- Used CFD to model catastrophic releases.

This paper presents a summary of the results of these studies. It also describes an improved (and partially validated) methodology for the characterisation of the source terms following a catastrophic vessel failure. This is achieved via a mathematical model known as airborne concentration estimate (ACE).

2. Background to catastrophic release modelling

2.1. Characteristics of a release due to catastrophic vessel failure

Storage vessels are designed to withstand the normal storage pressure, but may fail as a result of one or a combination of the following:

- an increase in internal pressure;
- a reduction in the strength of the vessel material;
- a local increase in loading.

Flawed material, fatigue, corrosion, poor manufacture and impact are all possible causes of failure. A more detailed discussion of the initiating events was given by Hurst [5] and Gould [6], who included quantification of the frequency of the different contributions to the risk of such events.

The sequence of events following the bursting of a vessel can be divided into a number of distinct phases:

- initial flash expansion, driven by the stored internal energy, leading to the formation of a fine aerosol and considerable turbulence;
- entrainment of ambient air due to the action of this turbulence, together with evaporation of the droplets, while the turbulence decays;

- gravitational slumping and reduction of the rate of entrainment of air in the presence of a stabilising density gradient;
- turbulent dispersion due to wind.

The focus of this paper is on the cloud formation phase (i.e. the release driven phase described by the first two steps above) rather than on the subsequent slumping and dispersion. No definitive criterion is available for the transition from the release driven stage to the subsequent dispersion stages, although this may be defined simply as the point where conditions match those assumed as input for the dispersion calculation. The output of any model of the formation phase can thus be seen as providing the input to the dispersion model.

The main stages in the development of a cloud containing vapour, droplets and air, arising as a result of the bursting of a vessel containing volatile material are shown schematically in Fig. 1. As containment is lost, the surface of the stored material is rapidly reduced from storage pressure (usually several bar) to atmospheric pressure. This reduction in pressure is transmitted through the liquid and thermodynamic equilibrium is lost. To regain equilibrium, some of the liquid boils to a vapour and the remaining liquid is cooled to its boiling point at atmospheric pressure. This forms vapour bubbles within the liquid, which expand as their pressure is reduced to atmospheric pressure. These rapidly expanding bubbles break up the remaining liquid into droplets which are thrown outwards and, together with the expanding vapour, form the cloud. As the liquid droplets are expelled, some impinge on the ground, possibly forming a pool, and the remainder break up, forming an aerosol.

The droplets within the aerosol then evaporate as air is entrained into the expanding cloud. Therefore the result of such an event is the very rapid formation (over a few seconds at most) of a large, cold and dense cloud consisting of air, vapour, and liquid droplets.

2.2. The risk context

The risk from sites storing pressurised materials can be quantified by assessing the consequences of a range of releases. The largest of these will be catastrophic releases, although their frequency is low. To demonstrate the importance of such events, example risk calculations were carried out. The example selected, which is the case studied by Carter et al. [7], considered chlorine as the hazardous material, and is representative of small chemical installations. The calculations are typical of those which would be carried out as part of a QRA of a major toxic hazard installation and demonstrate the process used by the Health and Safety Executive (HSE) in formulating hazard ranges. Full details are given by Gilham et al. [4] and the results are summarised here.

The events considered as part of the QRA range from the catastrophic failure of a storage vessel through to more probable, but less severe, events, such as pipe and flange failures. The example risk calculations demonstrated that large scale continuous releases dominate the risk, although instantaneous events become increasingly important in the far field. However, the effect of instantaneous releases will be enhanced where the installation is located within a building, or where other mitigation measures are in place, as this will significantly mitigate many of the continuous releases and hence reduce the risks from all events except catastrophic vessel failure [8].

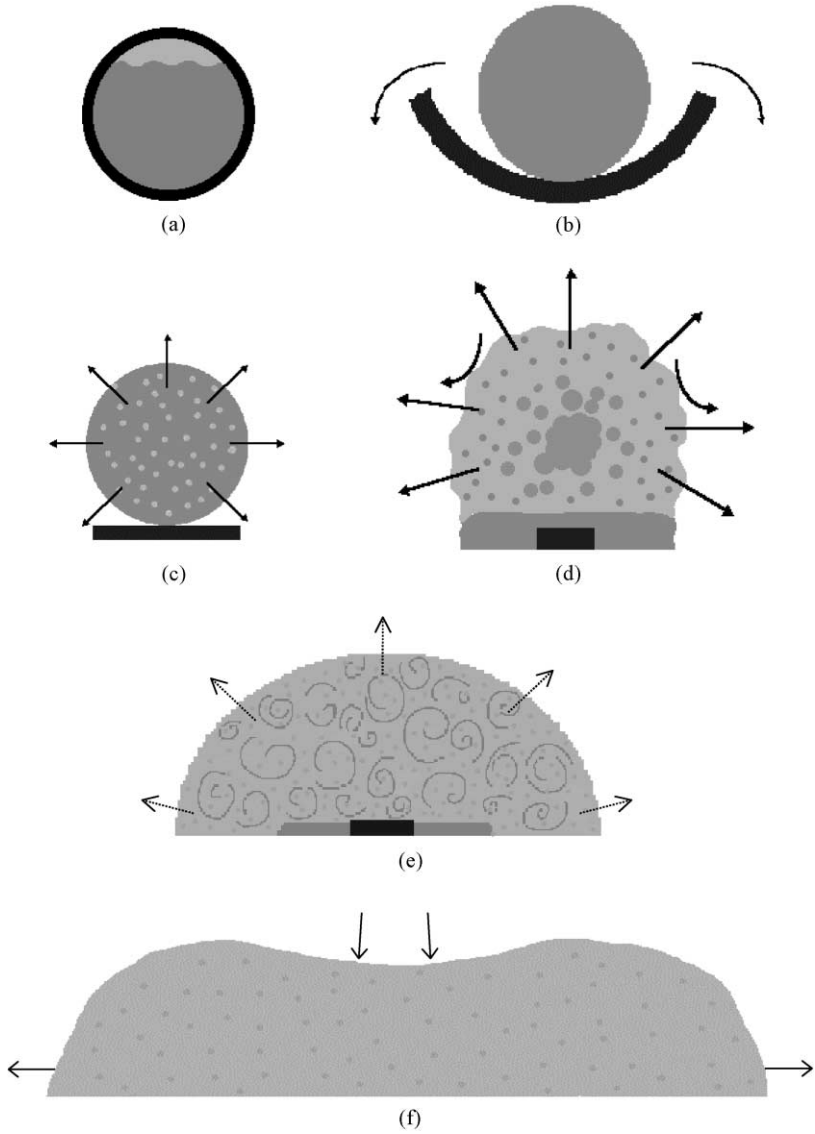

Fig. 1. Schematic illustration of the phases of a flashing release: (a) initial state; (b) loss of containment; (c) bubble nucleation and start of explosion; (d) explosive expansion, liquid break-up and air entrainment; (e) start of turbulence driven entrainment; (f) gravitational slumping, wind transport and further entrainment.

Sensitivity studies also revealed that the assumed duration of release of the total inventory of a large tank does have a significant effect on the calculated risks. It was found that, for both propane and chlorine, assuming a 10 min release gives greatly reduced hazard ranges compared with those calculated using shorter durations. Thus current US practice

[9], where it is assumed that a full inventory release over 10 min is a worst case, may therefore be non-conservative. These observations emphasise the importance of improving the understanding and modelling of large catastrophic instantaneous releases.

2.3. Current models

There are very few models which claim to describe such events, and those which do exist are all empirically based. Two of these, the TNO Yellow Book [10] and World Bank [11] models, are based on the experimental work of Hess et al. [12] and Maurer et al. [13]. These models adopt the approach of ignoring momentum and deducing the expansion velocity (assumed to be the same for the vapour and droplets) and the initial flash fraction from the steady flow energy equation assuming an isentropic expansion process.

Currently, within HSE, the IRATE3 [14] model, based on the method described in the Canvey Island report [15], is used for hazard range assessment. The mass of the entrained air is calculated empirically and is assumed to provide the heat necessary to vaporise the liquid droplets. The final equilibrium temperature, and hence the final vapour fraction, are then determined using a full enthalpy balance, on the basis that evaporation will continue until the partial pressure of the vapour is equal to the saturated vapour pressure of the released material. By assuming a particular aspect ratio of the resulting cloud, all the source terms required by a dispersion model can be determined.

Most of the available models are based on observations of small scale experiments, and little evidence exists that they may be used successfully beyond the bounds of the experimental data. Most experiments have been conducted for releases of much less than 1 t of the hazardous material, with the exception of the data of Johnson and Pritchard [16], where release sizes up to 2 t were considered. A parameter which may be particularly sensitive to scale is the amount of air entrained. In most models, this has been determined empirically from observations of the small scale experiments, and it may be limited at full scale simply by the availability of the surrounding air, and the rate at which it can realistically be drawn into the cloud.

3. CFD modelling

3.1. Overview

The formation of a two-phase cloud as a result of a catastrophic vessel failure is an extremely complex phenomenon, involving physical processes ranging from bubble nucleation and boiling through to turbulent entrainment and dispersion. Modelling the complete process thus represents a formidable challenge. The approach adopted was to consider the different phases of the release that are represented in Fig. 1, and gradually to increase the model complexity as each of the phases was better understood.

The CFD modelling started by considering the last two phases in the sequence of events (i.e. the turbulent growth and the slumping and dispersion phases) and then moved progressively earlier in the release sequence to consider the explosive expansion phase. The modelling did not, however, attempt to model the nucleation and boiling

processes, but has focused on events once the liquid mass has been shattered by the boiling process.

Detailed experimental data, suitable for validation purposes, are limited, and mainly provide information on the gross features of the cloud, such as its size. Therefore, the CFD models have been used primarily in a parametric fashion to investigate the different phenomena. However, two different applications, for which some experimental data are available, have been considered.

1. Freon-11 releases from a spherical flask [17].
2. Butane releases from a cylindrical tank [16].

3.2. Methodology

Full three-dimensional (3-D) CFD models were developed for both types of release considered, which, although differing in detail, both use the same methodology. All CFD simulations were carried out using the STAR-CD (version 3.05) general purpose CFD computer program developed by Computational Dynamics Ltd., UK. It solves the 3-D Reynolds averaged Navier–Stokes equations using an unstructured finite volume solver, and incorporates a variety of turbulence closure models. Fuller details of the CFD modelling are given in Gilham et al. [4]; a summary only of the salient features is given below.

The energy balance for a release from the initial conditions to the expanding cloud is illustrated in Fig. 2. The energy balance tracks the internal energy, kinetic energy and work done between the initial state (0) and the expanded state (1) (changes in potential energy are ignored). Initially, the stored material (assumed to be liquid) is at rest in the storage vessel and the total energy (E_0) at this point is given by the internal energy (U_0) at the storage conditions. The depressurisation is then assumed to follow an isentropic expansion path to pressure P_1. The flash fraction (X) is given by:

$$s_{\lambda 0} = X s_{\mathrm{g}1} + (1 - X) s_{\lambda 1} \tag{1}$$

where subscripts λ, and g denote liquid and gaseous states, respectively, subscripts 0 and 1 the initial and subsequent states and s the specific entropy. The liquid and gas mixture is assumed to be in equilibrium throughout and thus, for a particular pressure, the temperature is given by the saturation temperature.

The total energy at 1 is then given by

$$E_1 = E_0 - E_{\mathrm{a}} \tag{2}$$

where E_{a} is the work done in expanding the cloud and is given by

$$E_{\mathrm{a}} = P_{\mathrm{a}} \left(\frac{1}{\rho_1} - \frac{1}{\rho_0} \right) \tag{3}$$

where ρ is the density at the relevant state. The final specific kinetic energy, and hence expansion speed, is then given by:

$$\mathrm{KE}_1 = E_1 - U_1 \tag{4}$$

where U_1 is specific internal energy and KE the specific kinetic energy ($1.5\nu^2$).

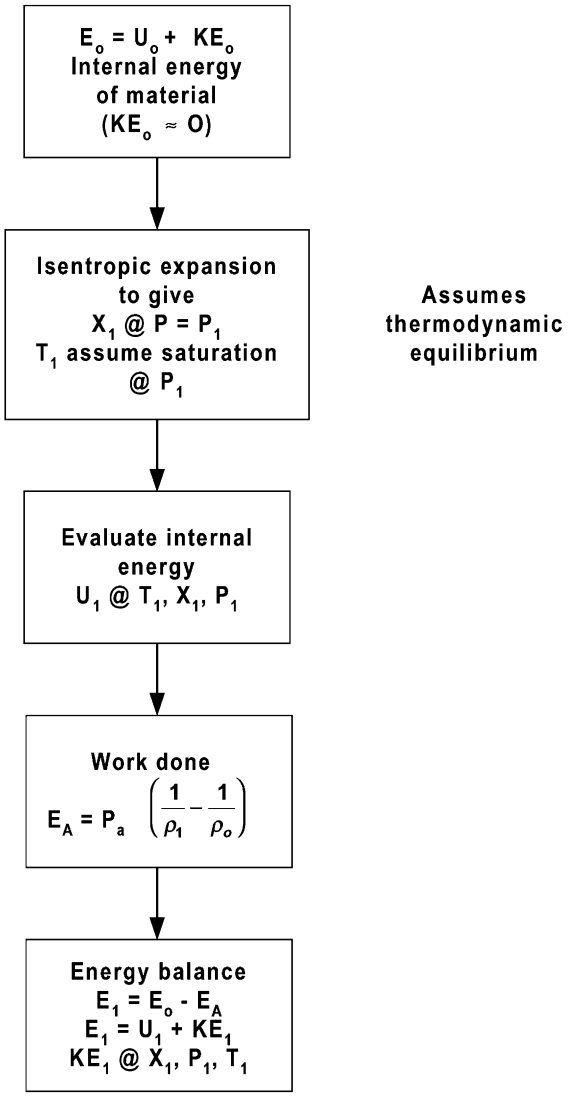

Fig. 2. Energy balance.

The resulting energy balance is used to calculate conditions at the end of the nucleation and boiling phase when the liquid has been shattered into droplets and a rapidly expanding vapour cloud has been formed. It provides the following initial conditions for the simulations:

- the vapour and droplet fractions;
- the velocity of the expanding cloud (vapour and droplets);
- the size and shape of the initial cloud.

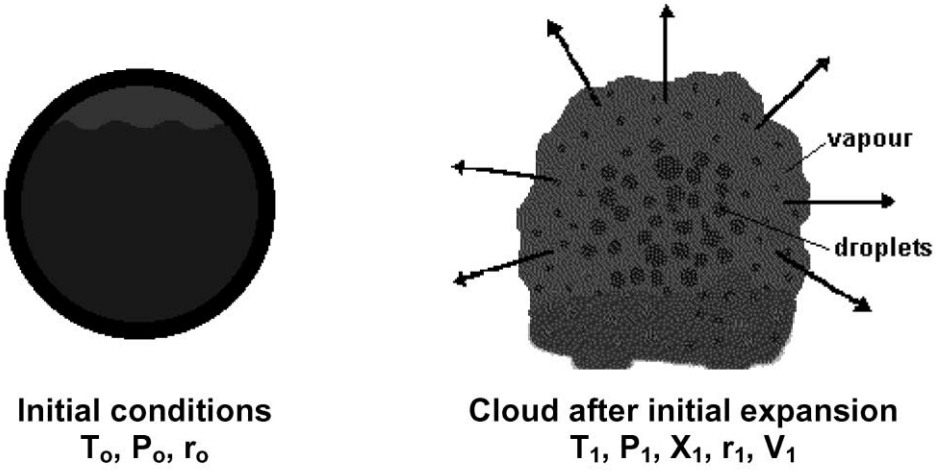

(a)

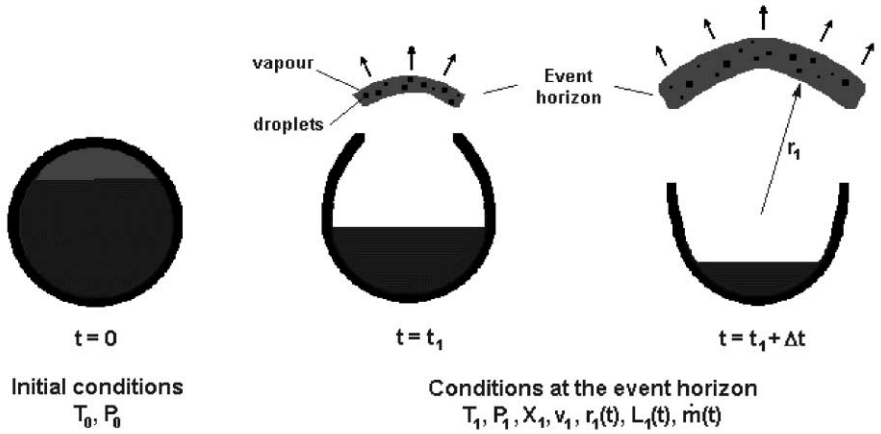

(b)

Fig. 3. Initial conditions: (a) flask simulations; (b) tank simulations.

Since the failure mechanisms differ, the application of these conditions varied between the two cases considered, as shown in Fig. 3. For the spherical flask experiments the initial conditions took the form of an instantaneous, uniformly expanding vapour and droplet cloud, whereas for the tank release, conditions were imposed as a time varying directional release.

The simulations were started after the initial nucleation and boiling process, and at a point when the liquid had been shattered to form an aerosol cloud. The released material was thus modelled as a large number of liquid droplets within a continuum of gaseous vapour. The mass, momentum and heat transfer between the two phases was calculated, as

was the turbulent motion of the droplets resulting from their interaction with the gaseous phase. The gaseous phase was assumed to behave as an ideal gas and the liquid phase as an incompressible liquid.

Simple assumptions regarding the temperature distribution inside the droplet are used to estimate the evaporation from the droplets. The average temperature of the droplets is higher than their boiling point once the surrounding pressure drops. Therefore evaporation is fast and the droplets effectively flash. The heat flow from the interior of the droplet to the surface is given by:

$$\dot{q} = 4\pi r_{\mathrm{d}} k_{\mathrm{d}} \Delta T \tag{5}$$

The resulting flashing rate, $\dot{m}_{\mathrm{d}}$, is given by:

$$\dot{m}_{\mathrm{d}} = \frac{\dot{q}}{h_{\mathrm{fg}}} \tag{6}$$

where r_{d} is the droplet radius, k_{d} the liquid thermal conductivity, h_{fg} the heat of vaporisation, and ΔT the temperature difference between the droplet and its surrounding environment. It is assumed that the surroundings consist of freon vapour at the vapour temperature. Once a droplet is surrounded by air instead of pure freon vapour, evaporation occurs due to the unsaturated nature of the air surrounding the droplet. Eq. (6) does not predict any evaporation at this stage. Therefore, once a droplet is surrounded by air, the standard model for droplet evaporation in STAR-CD is used [18,19]. This calculates the droplet evaporation in terms of the partial pressure of freon in the surrounding air, the velocity of the droplet relative to air and other properties of the materials and the flow.

The flow is assumed to be compressible, with the density varying with both temperature and pressure. Gravity is included in the calculation, as the vapour is dense. The effects of turbulence are modelled using the standard buoyancy-extended k–ε model [20].

3.3. Application to releases from a spherical flask

Pettitt [17] undertook detailed measurements of experiments involving flashing releases of pressurised freon-11 from spherical flasks which were smashed either mechanically or by an explosive charge. The sudden nature of the flask failure produced a release that was close to instantaneous and initially approximately symmetrical. A fraction of the liquid flashed off to form vapour immediately, shattering the remaining liquid to form an aerosol cloud and freon-11 vapour. Various properties of the vessel failure and the resulting two phase cloud were measured at frequent intervals after the release.

A number of experiments were conducted in which the fill volume of the flask, the internal pressure and the release substance were varied. A spherical flask was used for all the experiments and the internal pressure was varied by heating the saturated mixture in the flask. Simulations were made for a release from a 1-l flask containing 500 ml of freon-11 pre-heated to generate a pressure of 460 kPa. Although the release process is approximately symmetrical, after a few milliseconds, the freon cloud developed asymmetries which enhanced mixing. As it was considered important to be able to model these asymmetries, a full 3-D CFD model was developed.

The majority of the CFD calculations were carried out for the 1-l flask experiments described above. However, whilst carrying out the simulations it became clear that the predicted cloud development was sensitive to a number of the initial parameters. The model was therefore assessed to test the sensitivity of the results to the following initial parameters:

- initial velocity distribution within the cloud;
- initial pressure distribution;
- uniformity of the initial droplet and vapour velocities;
- initial flash fraction.

The development of the release showed slight asymmetry at 5 ms, with much clearer asymmetry at 50 ms. The variation of the cloud radius with time is shown in Fig. 4, in which two characteristic radii are used to define the edge of the cloud.

1. Cloud 1 is defined as consisting of regions in which the vapour (volumetric) concentration is greater than 10%.
2. Cloud 2 is defined similarly, but using the 1% concentration contour.

These results indicate that the cloud undergoes a rapid expansion followed by a short series of oscillations, after which the pressure within the cloud is approximately atmospheric. Subsequent expansion of the cloud, through evaporation and entrainment, is much slower than during the initial expansion to atmospheric pressure. This behaviour is supported by the observed behaviour in which the initial rapid expansion of the cloud was seen to 'halt' and to be followed by a much slower growth.

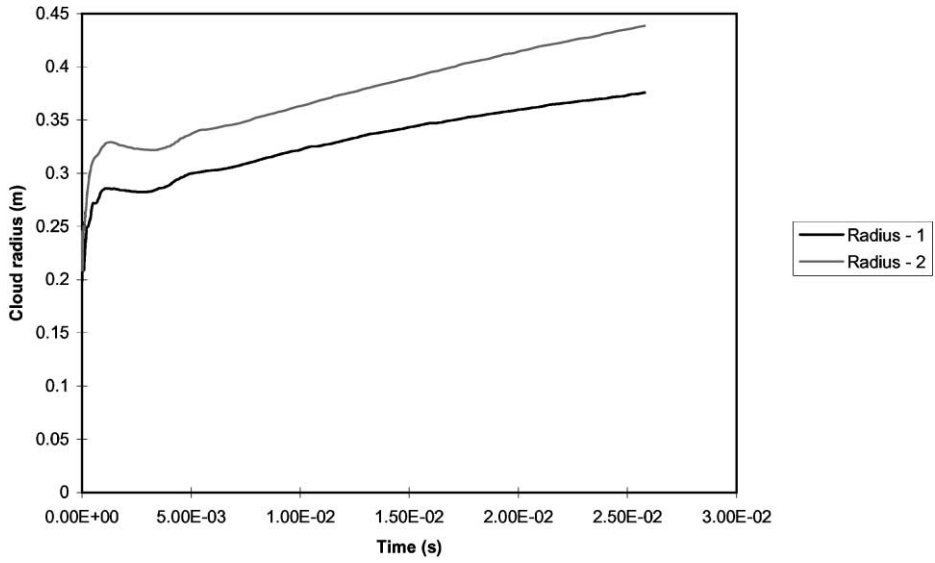

Fig. 4. Cloud radius vs. time for 1-l flask, calculated from volume within 10% (radius 1) and 1% (radius 2) concentration contours, respectively.

Comparisons were made between the CFD results and the experimental data, covering cloud edge velocity, droplet velocities and initial evaporation rate. Full details are given by Gilham et al. [4], and the following observations were made:

- the predicted cloud development was qualitatively similar to that observed experimentally;
- the initial velocity of the cloud edge was reproduced but the overall cloud size was under-predicted;
- the velocity of the liquid droplets was under-predicted by factors of around 1.5–3, with the discrepancies reducing as the transient proceeds.

Additional calculations demonstrated the sensitivity of the predicted cloud development to the imposed initial conditions; in particular, the predictions were shown to be sensitive to any asymmetry in the initial conditions and to the initial flash fraction. The initial flash fraction is determined by the thermodynamic path taken during the initial bubble growth and boiling stage of the release, and an isentropic expansion has been assumed for all calculations.

In addition to those for the 1-l flask, simulations were also carried out for similar releases from 10 l to 2.95 m^3 (2 t) flasks. These tests provided information on the dependence of the final cloud radius and velocity on the mass of the release. In these increased scale simulations, the geometry and conditions were kept exactly the same, as was the energy balance, so the initial velocity of the vapour and droplets was the same in the larger scale releases as in the 1-l case.

The shape of the cloud in each case was qualitatively very similar, and the traces of cloud radius and characteristic velocity with time for the larger cases were consistent with the profile for the 1-l case. The predicted variation of the cloud volume with the release mass is shown in Fig. 5, from which it is seen to be almost linear (the exponent of the variation is actually around 1.1). In contrast, the characteristic velocity remained effectively constant at around 5–6 m/s. These results suggest that the final cloud size is dependent on M, rather than on $M^{2/3}$ as used in the IRATE3 model. This dependence reflects the basis of the energy balance from which the initial cloud temperature, flash fraction and velocity were determined, and which has no mass dependence.

3.4. Application to releases from a cylindrical tank

Johnson and Pritchard [16] reported the results of a series of releases of 1 and 2 t of butane and propane from cylindrical tanks carried out at the Spadeadam test facility. The releases were ignited immediately after vessel failure, the main purpose of the tests being to provide information on the development of the ensuing fireballs. However, since the cloud was not ignited during the early development of the release, the tests also provide valuable information on the initial stages of a cold vessel failure.

Unlike the flask simulations, where the flask can be assumed to rupture ‘instantaneously’, and thus not to play any role in the flow development, the rupture of the vessel occurs over a longer timescale and does impact on the development of the release. Thus, for this application, the objective was to simulate the rupture of the vessel containing a flashing

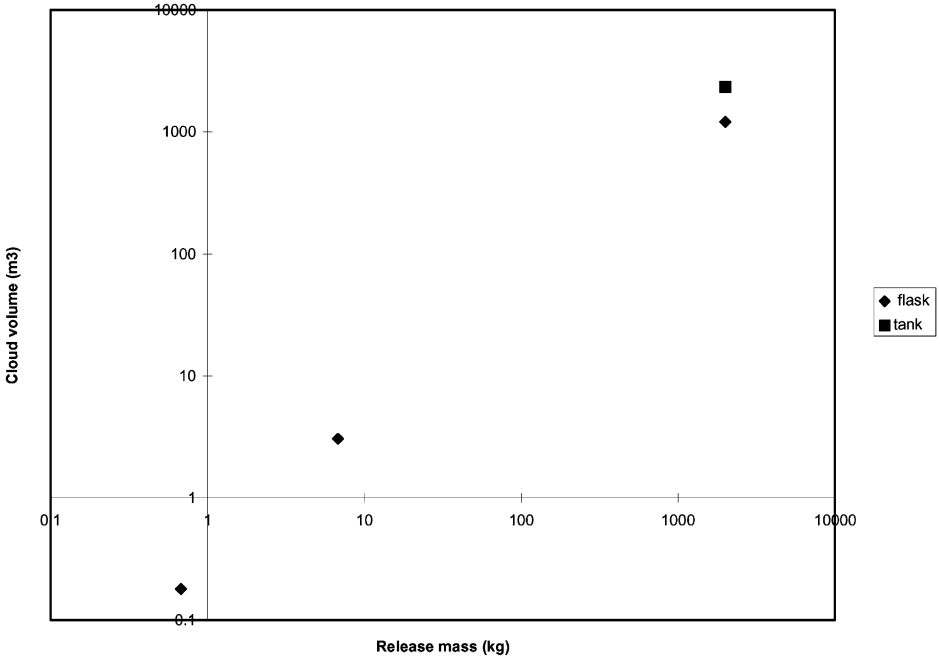

Fig. 5. Cloud volumes vs. initial mass for flask and tank simulations.

liquid in which the timescale of the rupture was comparable with the timescales of the initial flow development.

This required an extension of the modelling methodology used to simulate the flask experiments to include the following:

- a model of the time varying opening of the vessel (assumed to be a split running along the complete length of the tank);
- a time varying release rate from the vessel;
- a directional release, input into the CFD model at an 'event horizon', comprising an initial jet phase followed by a more uniformly radial release as the tank empties and opens fully.

The conditions at the event horizon were determined from the adiabatic depressurisation calculation within the energy balance. Simulations using the two phase jet model TRAUMA [21] indicated that the conditions at the opening would remain almost constant over the period of tank emptying despite the rapidly reducing pressure in the tank, such that at the opening the fluid comprises almost all liquid. The energy balance was therefore assumed to be constant over the period, so the vapour and droplet velocity and temperature at the event horizon remained constant for the complete duration of the tank opening.

The drop in pressure does, however, cause a reduction in flowrate per unit area through the opening during the tank emptying phase. The complex velocity–time curve was therefore

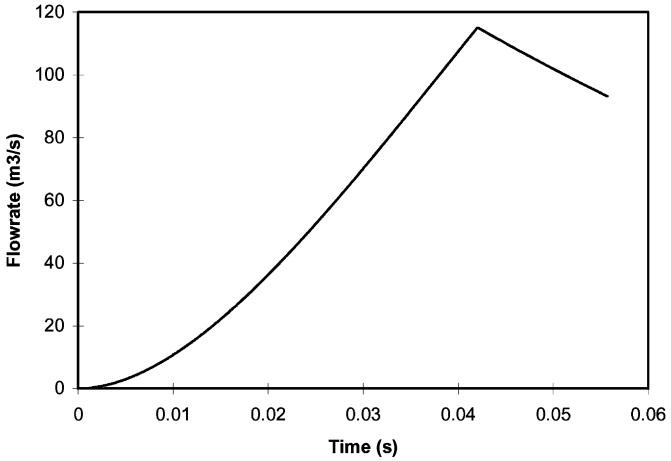

Fig. 6. Overall tank flowrate vs. time.

approximated by $V = 30–81.6\sqrt{t}$ (m/s). This flowrate, combined with the increasing opening, gave the total flowrate from the tank shown in Fig. 6.

As the initial conditions were assumed to be constant with time, the initial quality was maintained throughout at 0.597. Appropriate quantities of vapour and liquid in the form of droplets were injected with the same velocity (180 m/s) and temperature (276 K). There was little information on droplet sizes for this type of problem, and the empirical data are widely scattered. The Sauter mean diameter droplet size based on empirical data for sprays through orifices [22] was used to give the initial droplet size.

$$D_{\mathrm{d}} = 3.09\nu_{\mathrm{d}}^{0.385}(\sigma_{\mathrm{d}}\rho_{\mathrm{d}})^{0.737}\rho_{\mathrm{a}}^{0.06}\Delta P^{-0.54} \tag{7}$$

The STAR-CD droplet model [18,19] includes a droplet break-up model based on Weber number, such that stable droplets are those for which

$$We = \frac{\rho_{\mathrm{d}}(u - u_{\mathrm{d}})^2 D_{\mathrm{d}}}{\sigma_{\mathrm{d}}} \leq 12 \tag{8}$$

All droplets initially had the same diameter of 2.7×10^{-4} m. Because of the large volume of liquid expelled from the tank, implying a very large number of droplets, the technique of grouping the droplets together into parcels, as used in the flask simulations, was also employed. The number of droplet parcels injected at a given timestep was based on the volume flowrate of that timestep, with a lower bound to ensure a spread of droplets over the initial part of the tank opening. The number of droplets represented by each parcel was calculated dynamically to give the correct liquid flowrate for each timestep.

Fig. 7 shows the predicted cloud 0.07 s into the release. At this time the vessel is fully open and the cloud has developed its characteristic asymmetric shape. The cloud asymmetry is a consequence of the release mechanism and is consistent with the experimentally observed behaviour. The cross-sectional areas of the cloud in the simulation were 660 m^2

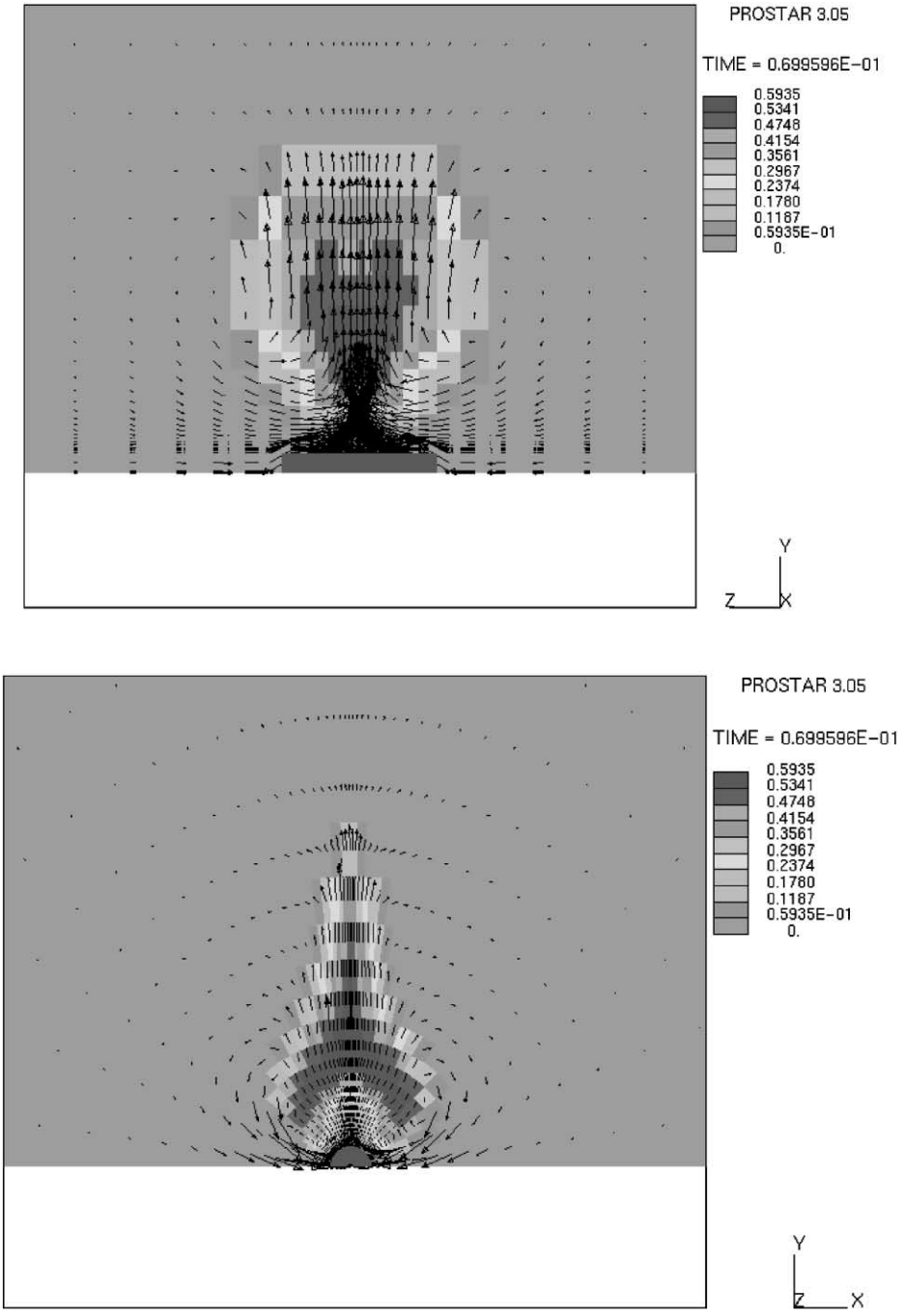

Fig. 7. Time $= 0.07$ s: concentration contours and velocity vectors on centreplane normal to tank axis (top); on centreplane parallel to tank axis (bottom).

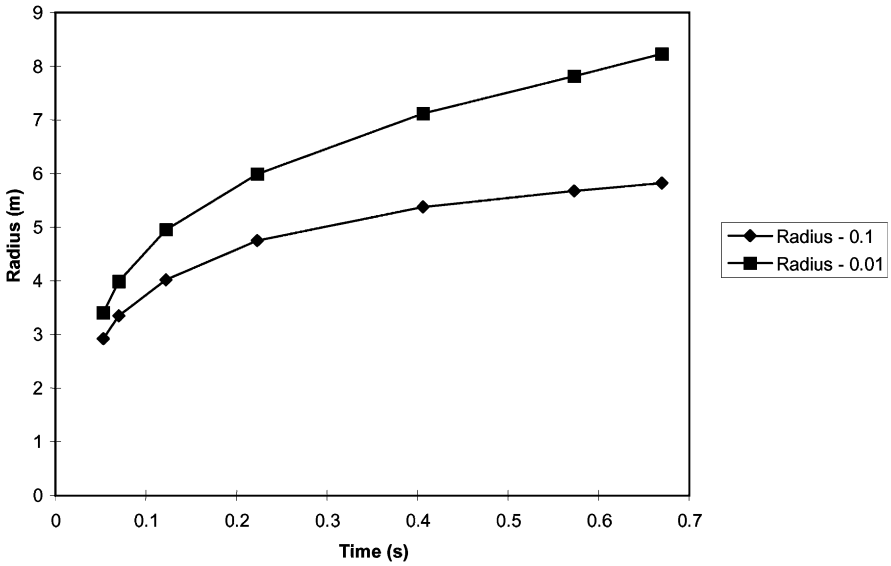

Fig. 8. Cloud radius vs. time for tank release calculated from the volume within the concentration contours (m^3/m^3) indicated.

in the direction normal to the tank axis and 1070 m^2 in the direction along the tank axis, giving an aspect ratio of 0.62. In the experiments, the size of the cloud was not measured, although the maximum size of the resulting fireball was. While the fireball was much larger than the cloud preceding it, the shape of the cloud remained similar. In the case modelled, the aspect ratio of the maximum fireball area for the equivalent ignited releases was 0.66.

The cloud 'radius', calculated assuming a spherical cloud, is shown in Fig. 8. In common with the flask simulations, there was an initial rapid growth in cloud size, during which time most of the droplets flashed or evaporated quickly, followed by an entrainment phase of much slower growth. The final cloud size, of 5.8 m for concentration greater than 0.1 and 8.2 m for concentration greater than 0.01, is close to that seen in the 2 t flask simulation, despite the different geometry, opening scenario and material; the predicted cloud volume is compared with the flask experiments in Fig. 5. The characteristic velocities were significantly higher in the tank opening case, being 19 and 10 m/s for cloud concentrations 0.1 and 0.01, respectively, compared with approximately 6 m/s for the flask.

3.5. Implications for the ACE model

Undertaking full 3-D CFD simulations has allowed considerable advances in the understanding of the behaviour of catastrophic releases. Although a versatile general-purpose CFD code was used for the simulations, considerable effort was required to develop appropriate sub-models to enable this type of release to be modelled. The CFD models have been used principally in a parametric manner, but, where data exist, direct comparison with

experimental data has provided confidence in the modelling approach. It is recognised, however, that this could not be considered to represent complete validation.

Underpinning the simulations is a detailed energy balance that has been used to provide initial conditions for the computations. Importantly, this highlighted the small proportion of the total energy that goes into the kinetic energy of the expanding cloud, and the sensitivity of this kinetic energy to the thermodynamic path assumed for the expansion process. A common modelling approach was used for both the flask and tank releases simulated, with the principal difference being the manner in which the initial conditions were specified. For the flask simulations, the initial conditions took the form of an instantaneous, uniformly expanding, vapour and droplet cloud, whereas for the tank release, conditions were imposed as a time-varying directional release.

A number of simulations of the 1-l flask (0.67 kg) experiments of Pettitt [17] were carried out. These showed a very rapid initial development of the cloud with oscillations, followed by slower growth due to entrainment. This supported the observed behaviour in which the initial rapid expansion of the cloud was seen to 'halt' and to be followed by a much slower growth. Additional calculations demonstrated the sensitivity of the predicted cloud development to the imposed initial conditions. In particular, the predictions were shown to be sensitive to any asymmetry in the initial conditions and to the initial flash fraction.

Two additional calculations were also carried out with initial masses of 6.7 and 2000 kg. The results of these predictions, shown in Fig. 5 (which also includes results for the tank simulation), indicated that the final cloud volume scales almost linearly with initial mass, and that the characteristic velocity within the cloud was independent of initial mass.

The predictions also indicated the importance of the tank in the development of the resultant cloud, showing that it both shapes the cloud and also generates large scale eddying motion within the cloud. The predicted clouds were also shown to be more energetic, larger and more dilute than those for the equivalent flask release case, suggesting that the release conditions do play an important role in determining the final cloud characteristics.

4. Development of a simple airborne concentration model

4.1. Structure of model

One of the objectives of this study was the development and validation of a practical method for the prediction of the ground-level concentration of material in the cloud. This was to be performed as a function of position and time during the phase represented by Fig. 1(f) (the slumping/transport phase). Since the slumping and transport are covered by standard dispersion models, the ACE model is intended to provide concentration and cloud size estimates at the beginning of this phase.

The ACE model employs two separate sub-models to cover the sequence illustrated in Fig. 1 and summarised in Table 1. Droplet modelling is also included in the turbulent growth phase. This considers that part of the cloud which is in aerosol form, and determines how its evaporation and subsequent behaviour modifies the cloud size, temperature and concentration.

Table 1
Characteristics of the ACE sub-models

Sub-model	Covers phases (Fig. 1)	Input	Output
Explosion	(a)–(d)	Storage conditions	Cloud state at end of explosive growth phase
Turbulent growth	(e)	Cloud state at end of explosive growth phase	Cloud state at end of turbulent growth phase

4.2. The explosion sub-model

The explosion sub-model is based upon the model described by Shield [23]. This model relies upon observations of early cloud behaviour, the most fundamental observation being that there exists a transition point where the main agent of cloud expansion appears to change from being the outwards momentum provided by the explosion, to the process of air entrainment due to inherent violent turbulence. The model assumes that, at this point, the state of the cloud bears a simple relationship to the initial conditions.

The explosion sub-model takes as its input the following data:

- material type;
- liquid mass;
- storage temperature and pressure;
- ambient temperature and pressure;

and without attempting to represent any of the intermediate processes, calculates the following characteristics of the cloud at the end of the explosion phase:

- cloud radius;
- masses of volatile material and of air;
- average cloud temperature;
- turbulent velocity and length scale.

The volume, V_c, of the cloud after phase 1 is given by the expression:

$$V_c = C\frac{XM}{\rho_{va}} \tag{9}$$

where M is the initial stored liquid mass of material (kg), X the fraction flashed to vapour upon depressurisation, ρ_{va} the vapour density at atmospheric pressure (kg/m^3), C a fitted constant.

From the constants presented by Shield [23], the value of C was derived to be 78, i.e. the cloud volume is equal to 78 times the flashed vapour volume. Although this value of C gave predictions of V_c which were consistent with observations, it was found that improved fits could be obtained, to both observations and CFD simulations, by taking a slightly lower value, of around 57. This re-interpretation was introduced, because it is possible for an observer to be in error both in the volume estimate and in the identification of what constitutes the end of the explosion phase (which in reality is not completely distinct from the subsequent turbulent growth phase). This suggests that those cloud volumes which were interpreted as applying to the end of the explosion phase could instead be assumed to apply

to some point within the turbulent growth phase, implying that the volume produced by the explosion phase alone would actually be somewhat smaller. For example, the end of the explosion phase could be taken at the time when the first maxima are reached in Fig. 4, or within a short period prior to this when the slopes of the curves have decreased.

The explosion phase produces a highly turbulent cloud, which continues to entrain air rapidly until the turbulence diminishes to levels where standard dense gas dispersion models can predict the subsequent behaviour. The turbulent velocity u_L at the end of the explosion phase was given by Shield [23] as:

$$u_L = 40 \left(\frac{X \rho_a^2}{\rho_{va} \rho_{sva}} \right)^{1/9} \text{m/s} \tag{10}$$

where ρ_a is the air density (kg/m^3), ρ_{va} the vapour density at ambient temperature and pressure (kg/m^3), ρ_{sva} the saturation vapour density at the ambient temperature (kg/m^3).

Because of the small value of the exponent in Eq. (10), u_L tends to lie between 25 and 35 m/s for all practical situations. For an intermediate scale release (a few tonnes), the growth arising from the initial turbulence at this level can increase the cloud volume by a factor of typically 5–10.

The turbulent velocity predictions from CFD are in the range from 6 m/s for a spherically symmetric release to 19 m/s for a directed release. With the current evidence, the value of u_L adopted can be considered to be independent of initial mass, with 10 m/s being suggested as a typical value. However it may be expected to vary somewhat with the degree of symmetry in the direction of the release. The explosion sub-model includes the assumption that a multiple of the flashed mass becomes airborne (to a maximum airborne fraction of 1.0). This is based upon freon release data from Bettis [24], which are reproduced in Fig. 9, and which show a fair degree of scatter. Although it is understood that the same failure mechanism was used for all the tests, it is assumed that at least some of the scatter can be taken to be representative of the effects of release direction, the two options being as follows.

1. Downward
   If the vessel failure is initiated near the bottom, the pressurised vapour at the top of the void will force the liquefied gas downwards, reducing the quantity of airborne material.
2. Omni-directional
   If the failure is located in the upper regions of the vessel, the vapour does not have the same effect as above, and material will be scattered in all directions, producing a much higher airborne fraction.

On this basis, the correlations shown in Fig. 9 were developed to represent these differences.

4.3. The turbulent growth model

Standard methods exist for the prediction of slumping, transport and dispersion of dense clouds, on the assumption that the cloud is quiescent, with no initial internal turbulence. Therefore, in order to use one of these standard methods, it is first necessary to take the

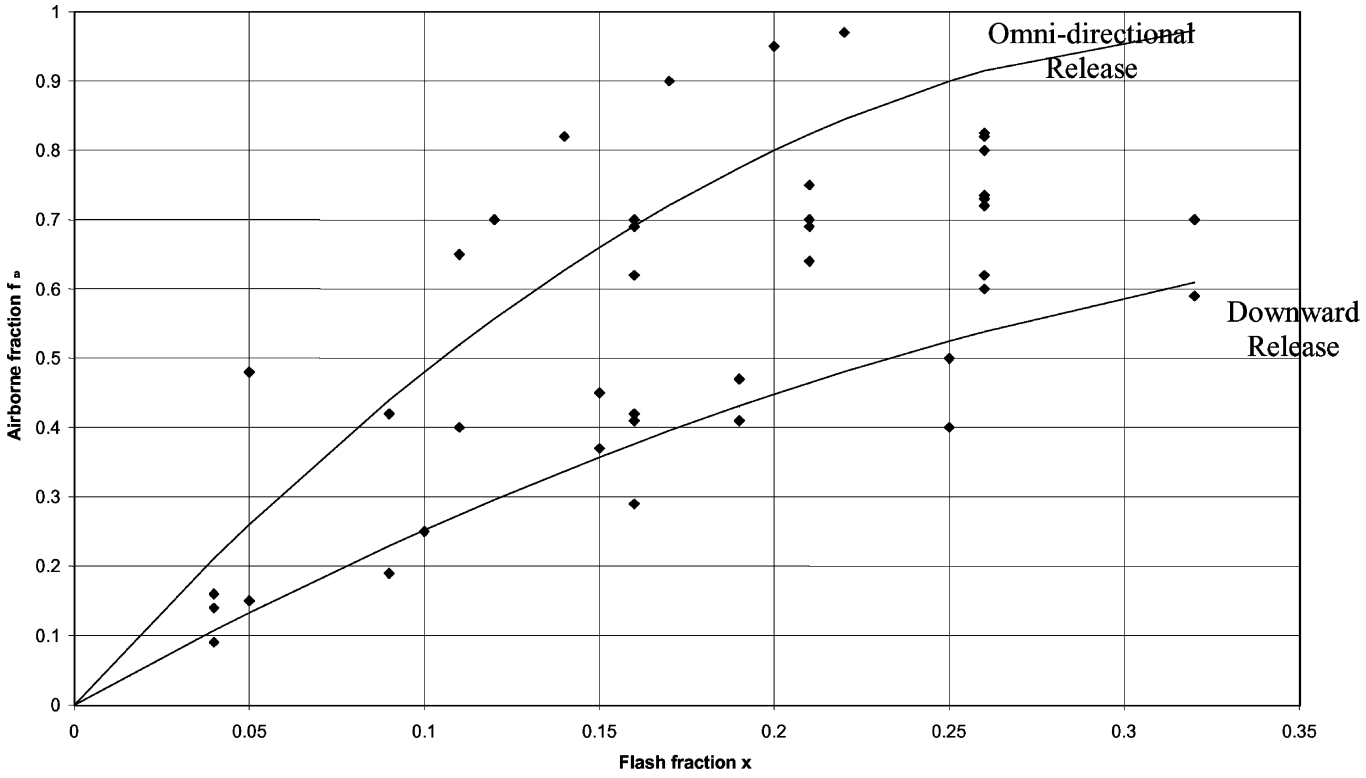

Fig. 9. Airborne fraction correlations.

cloud state at the end of the explosion phase and predict the state arising when the initial turbulence has decayed to a level comparable with the sum of the atmospheric turbulence and any turbulence created by slumping. The assumption of the ACE model, that slumping does not occur to a significant extent until after the turbulent growth phase is over, can be justified only if this phase is sufficiently short; say $\leq$10 s. On the basis of the simple model used to predict turbulent growth, this is almost always the case.

Turbulence decay can occur by dissipation, and by dilution. The former is represented by the homogeneous k–ε model and the latter by the assumption that the rate of growth of the edge of the cloud is proportional to the mean turbulent velocity, leading to a set of three simple differential equations which are solved numerically:

$$\frac{\mathrm{d}k}{\mathrm{d}t} = -\frac{bk^{3/2}}{r} - \varepsilon \tag{11}$$

where ε is the rate of energy dissipation due to viscosity (J/kg/s), r the characteristic radius of the cloud (m), b a dimensionless constant.

The variation of cloud radius is given by

$$\frac{\mathrm{d}r}{\mathrm{d}t} = \frac{b}{3}k^{1/2} \tag{12}$$

and the variation of ε is determined by the equation:

$$\frac{\mathrm{d}\varepsilon}{\mathrm{d}t} = -\frac{C_{2\varepsilon}\varepsilon^2}{k} \tag{13}$$

where $C_{2\varepsilon}$ is a dimensionless constant.

The values of b and $C_{2\varepsilon}$ were derived by fitting the results to one of the CFD calculations of the development of the cloud arising from a 30 t chlorine release. The fitted values are:

$$b = 1.0$$

$$C_{2\varepsilon} = 2.1$$

The value normally quoted [25] for $C_{2\varepsilon}$ is 1.92, so this slight adjustment is considered to be not unreasonable. The value of b of 1.0 implies that the cloud edge grows outwards at a rate of about 40% of the mean turbulent velocity. The fitted value of b is therefore also judged to be plausible. The calculation for the case used for the parameter indicates that the turbulent growth phase can be considered to be completed in less than 5 s, well within the time limit referred to above for the validity of the model.

The initial conditions for these equations can be obtained from the cloud volume, turbulent length scale and turbulent velocity at the end of the explosive phase. The turbulent growth phase is considered to be over when the turbulent kinetic energy has fallen to a value equal to that which would be generated by gravitational slumping.

4.4. Droplet modelling

Throughout the explosion phase, a proportion of the material forms an aerosol within the cloud. During the turbulent growth phase, droplets within this aerosol are subjected to

evaporation due to air entrainment and at the end of this phase, any droplets remaining may rain-out, thus modifying the cloud conditions.

This aerosol is assumed to be represented by a range of droplet sizes which are log-normally distributed [26,27]. The standard deviation is taken as 1.8, which is consistent with data provided by Reist [26], and the mean diameter is a function of superheat, determined from the data of Johnson and Woodward [27]. These data also demonstrated a slight dependence of mean diameter on overpressure (higher pressure causing smaller droplets due to increased attrition during the explosion phase) and this is also incorporated.

Having established the initial droplet size distribution, it is then necessary to determine the characteristics of the droplet evaporation, which is caused by the entrainment into the cloud of air at a higher temperature. The heat transfer mechanism for each individual droplet is calculated by assuming that it evaporates in such a way that its volume reduces at a rate proportional to its surface area. It can then be shown that this implies a constant rate of reduction in droplet diameter, with the constant of proportionality being determined from the heat flux per unit area, liquid density and latent heat of vaporisation.

Liquid density and heat of vaporisation are assumed to have constant values, whereas the heat flux per unit area may be calculated via the heat transfer coefficient and the degree of superheat in the droplets at the moment they are exposed to atmospheric conditions. The superheat is calculated from the storage conditions and the heat transfer coefficient is calculated via a function of the Nusselt number, as given by Whitaker [28]. The Nusselt number correlation is dependent upon the Reynolds number, which is a function of the droplet velocity, which in turn is a function of the drag coefficient. As the drag coefficient is a function of the Reynolds number, an iterative approach was employed to achieve converged values for each variable.

By plotting the initial droplet size against the drag coefficient, it was found that the drag coefficient could be represented as a function of droplet diameter. For a given droplet size, this formulation of drag coefficient is used to produce values for droplet velocity and the Reynolds number, giving sufficient information to calculate the Nusselt number and heat transfer coefficient, and subsequently the heat flux per unit area. Hence the rate of reduction of droplet diameter may be established. Hence, it was found that droplets with an initially small diameter evaporate completely during the turbulent decay phase, whilst larger droplets reduce in size.

4.5. Modelling options

The ACE model produces output relating to cloud size, composition and temperature at the end of the turbulent growth phase. The liquid pool, aerosol and vapour components can then be used within dispersion models to calculate the subsequent cloud behaviour, and hence to calculate hazard range and risk.

It may on occasion be considered appropriate to simplify the output, for example, to be able to use a dispersion model which did not allow for aerosol effects, or to use worst case assumptions for the evaporation of any pool. Thus, at the end of the turbulent growth phase, there are 10 possible scenarios concerning the fate of any remaining droplets and pool mass, as summarised in Fig. 10, which also indicates which phases (liquid pool, aerosol, vapour) will appear in the final ACE output.

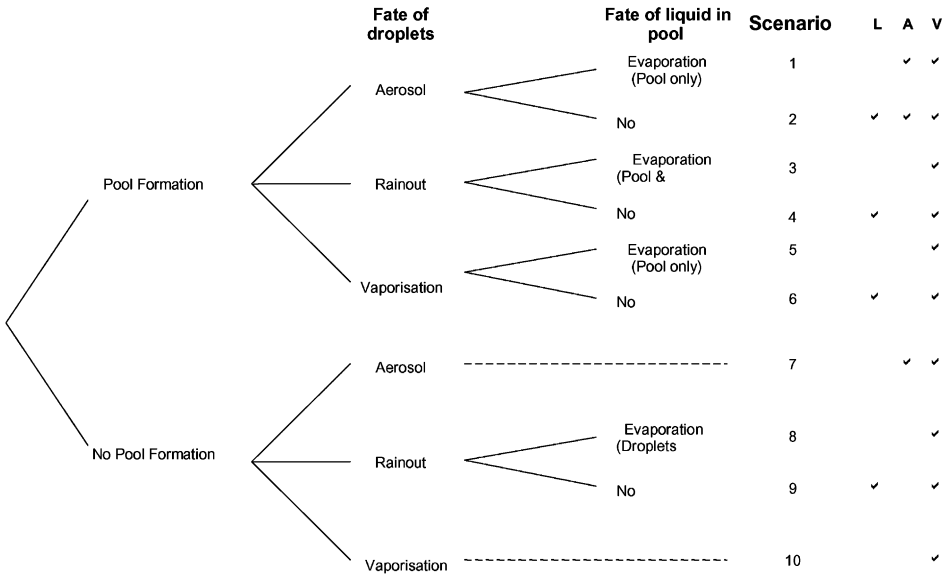

Fig. 10. Possible droplet and pool fates.

Each of these scenarios results in an updated cloud temperature and in some cases (vaporisation) a new mass of entrained air. Hence revised enthalpy balances and ideal gas relations are provided for each event to enable cloud temperature and entrained mass of air to be calculated.

The various options identified in Fig. 10 are implemented in three stages.

1. Pool formation

   This refers to *initial* pool formation, and is independent of any subsequent droplet rain-out at the end of the turbulent growth phase.
2. Fate of droplets

   At the end of the turbulent growth phase, a proportion of the mass is predicted to be in the form of an aerosol in the cloud. The following options are available.
   - Aerosol: droplets remain as aerosol.
   - Rainout: droplets added to existing pool, or form new pool.
   - Vaporisation: droplets totally evaporated by the entrainment of sufficient extra air.
3. Fate of liquid pool

   If there is any material within a liquid pool, the user has the option to specify that this should be evaporated into the cloud at the end of the turbulent growth phase. In this case, it is assumed that all the heat required is drawn from the pool substrate, and the material enters the cloud at its boiling point with no additional air entrainment.

5. Model validation

5.1. Validation base for ACE predictions

Although several experimental studies of catastrophic flashing releases have been carried out, the number of published observations suitable for model validation purposes is surprisingly small, as few studies report observations of cloud dimensions in sufficient detail. Experiments from which cloud volume measurements were made (or can be inferred) can be divided into two categories.

1. Small scale ($\leq$1 kg of material).
2. Medium–large scale ($\sim$100–1000 kg).

Fig. 11 reproduced from Maurer [13] shows the expansion of a cloud of propylene vapour and droplets, arising from an initial mass of 0.124 kg at an initial temperature of between 50 and 80°C (the temperature corresponding to the figure is not stated unambiguously in the reference).

Further validation is provided by the observations of Pettitt [17], concerning the cloud size following the shattering of a suspended spherical glass vessel containing 0.74 kg of freon-11 at a temperature of about 80°C. Pettitt states "... the aerosol cloud reached a distance of approximately 1 m from the 1×10^{-3} m^3 vessel in the vertical direction and approximately 0.8 m in the horizontal". The original ACE explosion sub-model predicted a radius of 0.91 m for a spherical cloud and the model with modified parameters (see Section 5.3) gave 0.82 m.

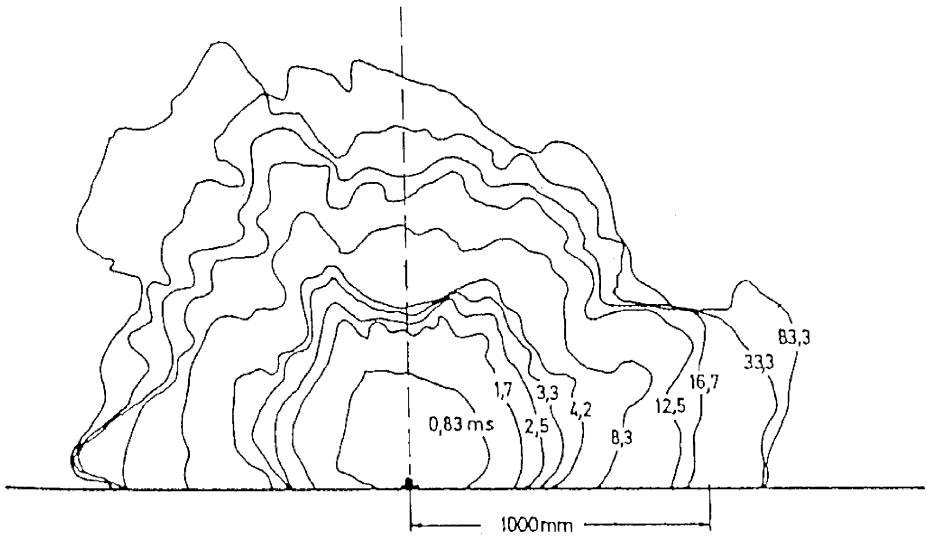

Fig. 11. Explosion phase of propylene release ($M = 0.124$ kg) from the small scale experiments of Maurer et al.

The predictions of the model are also qualitatively consistent with the experimental observations made by Hess et al. [12] and by Schmidli et al. [3]. However, in neither of these documents are measurements reported which can be compared directly with the radii predicted by the explosion sub-model.

The model upon which the explosion sub-model was closely based was derived from and fitted to the British gas experiments carried out at Spadeadam, and it is reasonable to assume that the model should therefore reproduce the results of these large scale experiments fairly well. However, it should be noted that it was not possible to derive cloud volumes from the video of these experiments, and hence to confirm independently the predictions of the model.

The only other experiment of this scale for which it appears that there are measurements of cloud size were those reported by Hardee and Lee [29]. In these experiments, the release of the material was not due to total loss of containment, but took place via an orifice in the tank. Nevertheless, the releases were sufficiently rapid that they can reasonably be compared with the predictions of a model which assumes total instantaneous loss of containment. Fig. 12 shows the variation in cloud radius with time as observed by Hardee and Lee, compared with the radius (broken line) calculated for the end of the explosion phase by the ACE

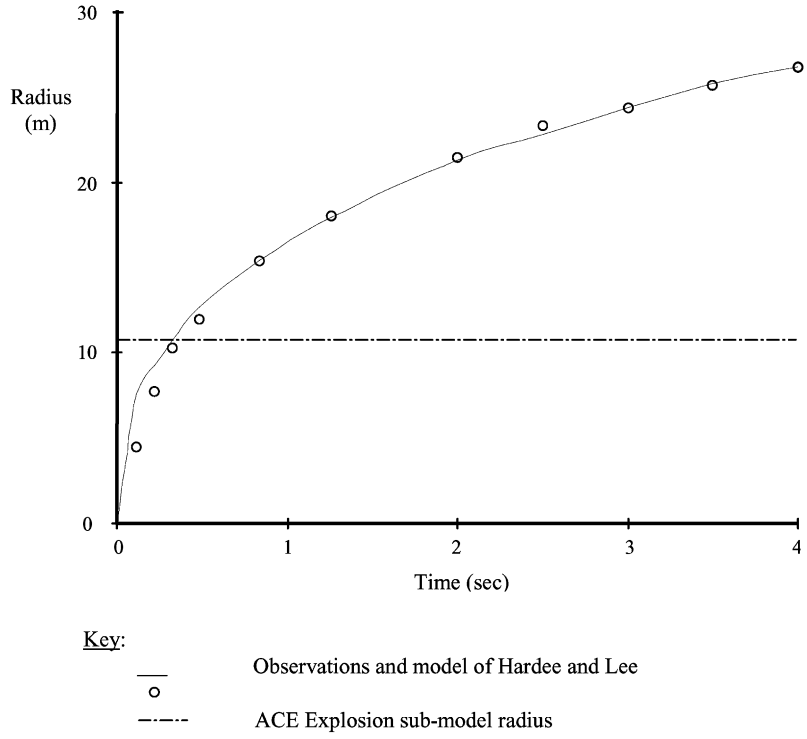

Fig. 12. Comparison of ACE explosion sub-model predictions with observation for release of 421.8 kg of propane: (-o-) stands for observations and model of Hardee and Lee; (– – –) for ACE explosion sub-model radius.

model. It is considered that the two are consistent, given the differences between model and experiment referred to above.

Although they cannot provide complete validation, these published measurements provide encouraging support for the predictions of the explosion sub-model at the end points of a large range (10–10^3 kg) of initial masses. As discussed in Section 3.3, this tends to suggest that the volume of the cloud at this stage in its development is proportional to initial mass M, in contrast to some models (e.g. the IRATE3 model) which assume that volume is proportional to $M^{2/3}$.

5.2. Information from CFD results

The CFD calculations described in Section 3 provide information and improved understanding in a number of areas where support from theoretical considerations or experimental observations is weak. In particular, the results have been used to help provide answers to the following questions.

1. Is there a well-defined end to the explosion phase?
2. How does the cloud radius at the end of the explosion phase vary with the initial mass of material?
3. What gives rise to the turbulence at the end of the explosion phase, and is the method of release important in determining the level of turbulence?
4. For a given method of release, how does the resulting turbulent velocity vary with initial mass?

Relevant information for most of these areas was extracted from the simulations of the shattered spherical flask experiments, as reported in Section 3.3. In these calculations, the experimental release of 0.67 kg of heated freon-11 was simulated. The size of the release was then scaled up to represent initial masses of 6.7 and 2000 kg.

5.2.1. Explosion phase

The variation of cloud radius with time for the case of a 1-l flask (containing $M = 0.67$ kg of freon-11), as calculated by CFD, is shown in Fig. 4, in which 'radius-1' gives the size of the cloud to the 10% concentration contour, with 'radius-2' corresponding to 1% concentration. For this method of release, which is almost spherically symmetric, there is clearly a point at which the initial explosive expansion almost comes to a 'halt', and is followed by a much slower growth. These results, together with the observational evidence reviewed previously, confirm that the treatment of the initial expansion as a distinct phase is realistic.

5.2.2. Cloud radius

The variation of cloud radius with initial release mass has been discussed in Section 3.3. It was shown in Fig. 5 that the scaling was almost linear (also see comments at end of Section 5.1).

5.2.3. Turbulence velocity

Fig. 13 shows a representation of turbulent velocity at the end of the explosion phase, as a function of initial mass. The value of around 5–6 m/s is essentially constant, but is

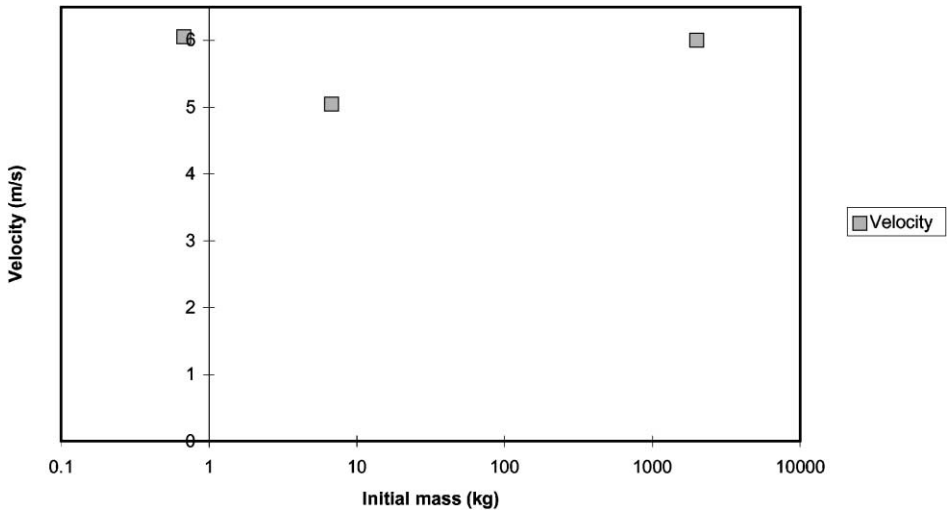

Fig. 13. Flask final cloud velocities as a function of initial cloud radius, from CFD flask simulations.

clearly somewhat lower than the value of around 24 m/s predicted using the original model of Shield. However, for this quantity, there are no experimental observations with which to compare the predictions. In addition to the spherical release simulations, CFD was used in order to represent the slower and more directional type of release as produced in the Spadeadam tests. The calculations represented the release of 2000 kg of heated (377°K) butane, with the characteristics of the release being taken from observations of the video of the experiment. The CFD prediction for the turbulent velocity for this release ranges from 10 to 19 m/s, depending upon assumptions. This is significantly higher than those predicted for the spherical releases and, despite the (possible) under-prediction of cloud volume, this does suggest that the amount of turbulence generated in the cloud is dependent upon the characteristics of the release (this is common for questions 3 and 4).

5.3. Refinement of model constants

If the model constants suggested by Shield were used, then ACE would significantly over-predict the cloud volume and the turbulent velocity. However, in contrast to the case for cloud volume, the ACE prediction of turbulent velocity has little theoretical and very limited experimental support, and it is considered that the CFD models may give a reasonable estimate of this quantity.

The turbulent velocity as calculated within ACE was therefore reduced to a level consistent with the predictions of the CFD results reported in Section 3. With the current evidence, the value adopted can be considered to be independent of initial mass, although it may be expected to vary somewhat with the degree of symmetry in the direction of the release. It was therefore determined that, until further evidence becomes available, a value of 10 m/s is appropriate.

A second way in which conservatism could be introduced is via a re-interpretation of the experimental cloud volume data, which is necessary because of the potential for observational 'error', as discussed in Section 4.2. It is therefore suggested that those cloud volumes which had been interpreted as applying to the end of the explosion phase could instead be assumed to apply to some point within the turbulent growth phase, implying that the volume produced by the explosion phase alone would actually be somewhat smaller. The extent to which the constant C in Eq. (9) should be reduced is determined largely by the degree of conservatism which it would be appropriate to introduce. It is suggested that a reduction by 25% remains consistent with observation (the corresponding reduction in radius would be about 10%). The modified ACE results are shown in Fig. 12, where they are compared with the Hardee and Lee observations [29].

6. Model sensitivity

6.1. Released material

The base case is taken to be the loss of containment of a vessel containing 1000 kg of chlorine at its saturation pressure at an ambient temperature of 288 K. The ambient pressure, wind speed and Pasquill stability are set at 101,325 N/m^2, 5 m/s and D (neutral), respectively. The vessel is on an industrial site with a roughness length of 0.1 m and will fail so as to produce an omni-directional cloud with an initial turbulent velocity of 10 m/s. The formation of a pool will be allowed and at the end of the turbulent growth phase any residual droplets will be allowed to remain as an aerosol within the cloud.

By retaining all other base case model parameters, the model was re-run with propane and ammonia. Results from these sensitivity runs are compared in Table 2.

Table 2
Material sensitivity comparison

Parameter	Base case		
	Chlorine	Propane	Ammonia
Vapour mass (kg)	723	938	739
Cloud radius (m)	13.42	20.78	24.23
Cloud temperature (K)	276.02	282.48	278.21
Concentration (m^3/m^3)	1.98×10^{-2}	1.07×10^{-2}	1.43×10^{-2}
Aerosol fraction	1.22×10^{-3}	0	2.45×10^{-4}
Airborne mass (kg)	1.34×10^{4}	4.73×10^{4}	7.51×10^{4}
Pool mass (kg)	260	61.6	242
Pool diameter (m)	13.42	20.78	24.23
Mass of air (kg)	1.26×10^{4}	4.63×10^{4}	7.43×10^{4}
Droplet mass (kg)	16.3	0	18.4
Cloud volume (m^3)	1.01×10^{4}	3.76×10^{4}	5.96×10^{4}
Velocity (m/s)	4.05	4.46	4.58
Duration of transient[a] (s)	2.31	3.58	6.52
Distance travelled (m)	4.68	8.00	14.93

[a] Time before onset of slumping.

Table 3
Release size sensitivity comparison

Parameter	Base case		
	1 t	10 t	100 t
Vapour mass (kg)	723	7330	73200
Cloud radius (m)	13.42	26.27	50.48
Cloud temperature (K)	276.02	272.03	266.04
Concentration (m^3/m^3)	1.98×10^{-2}	2.67×10^{-2}	3.76×10^{-2}
Aerosol fraction	1.22×10^{-3}	6.97×10^{-4}	1.06×10^{-3}
Airborne mass (kg)	1.34×10^{4}	1.03×10^{5}	7.59×10^{5}
Pool mass (kg)	260	2600	26000
Pool diameter (m)	13.42	26.27	50.48
Mass of air (kg)	1.26×10^{4}	9.56×10^{4}	6.85×10^{5}
Droplet mass (kg)	16.3	71.8	801
Cloud volume (m^3)	1.01×10^{4}	7.59×10^{4}	5.39×10^{5}
Velocity (m/s)	4.05	4.59	5.09
Time before onset of slumping (s)	2.31	2.97	3.24
Distance travelled (m)	4.68	6.83	8.25

Both the propane and ammonia releases took longer than the base case (chlorine) for the turbulence to dissipate; as a result, all propane droplets evaporated into the vapour phase giving a zero aerosol fraction, whilst a residual ammonia droplet mass remained in a larger cloud, giving a smaller aerosol fraction than in the base case. The clouds for both sensitivity cases have slightly higher temperatures than the base case, due to the greater volume of air entrained. In both cases, the cloud centroid travels with a higher velocity than in the base case (because of the greater cloud size) and as a result each cloud moves a greater distance downwind. All differences may be accounted for by the material properties.

6.2. Release size

To evaluate the sensitivity of the size of release, storage masses of 10 and 100 t (10,000 and 100,000 kg, respectively) of chlorine were used as inputs, generating the results given in Table 3.

Even though the time to achieve non-turbulent cloud conditions is longer for larger releases, and larger quantities of air are entrained, the resulting clouds become more concentrated. For all three scenarios, droplets remain with a slightly lower aerosol fraction for the 10 t release than for the others. The larger clouds are cooler than in the base case, due to the increased initial temperature drop and an insufficient quantity of air to provide the required heat transfer to restore ambient conditions.

6.3. Release direction

This section compares results for the two alternative release directions. Omni-directional and downward release directions invoke spherical and hemi-spherical cloud geometries, respectively, and results from this sensitivity study are presented in Table 4.

Table 4
Release direction sensitivity comparison

Parameter	Base case	
	Omni-directional	Downwards
Vapour mass (kg)	723	390
Cloud radius (m)	13.42	12.69
Cloud temperature (K)	276.02	276.48
Concentration (m^3/m^3)	1.98×10^{-2}	2.52×10^{-2}
Aerosol fraction	1.22×10^{-3}	2.98×10^{-3}
Airborne mass (kg)	1.34×10^{4}	5.71×10^{3}
Pool mass (kg)	260	593
Pool diameter (m)	13.42	12.69
Mass of air (kg)	1.26×10^{4}	5.31×10^{3}
Droplet mass (kg)	16.3	17.0
Cloud volume (m^3)	1.01×10^{4}	4.28×10^{3}
Velocity (m/s)	4.05	2.97
Time before onset of slumping (s)	2.31	1.71
Distance travelled (m)	4.68	2.55

The initial airborne fraction is greatly influenced by the release direction (see Section 4.2), with a smaller fraction being generated for downward releases. This means that a higher proportion of the pollutant will enter the pool, and the cloud volume is subsequently smaller. As the cloud is smaller, less air is entrained to evaporate the droplet mass, resulting in a higher residual droplet mass and hence aerosol fraction. This also produces a higher cloud concentration than in the omni-directional release.

7. Conclusions

The review of phenomenology identified the various stages of a catastrophic release, and demonstrated the complexity of the processes involved. The main problems in modelling the release arise in the rapid transition from a liquid mass in which bubbles form and grow, to a vapour cloud in which droplets of various sizes are moving at speed, breaking up and vaporising. In view of this complexity, current models are relatively crude and take little account of the fine detail of the physical processes which are taking place. The results are therefore effectively based on the extrapolation of results from small to larger scales. The greatest uncertainty which then arises is whether the 'final' cloud volume scales as $M^{2/3}$ or as M, where M is the initial stored liquid mass.

Various stages of the process under consideration have been modelled using CFD. Since current general purpose CFD codes do not include sub-models to cover all stages being considered, it has been used carefully to cover just some of the stages of the process. In addition, sub-models have been developed to enable CFD to be applied over a greater part of the problem. The 3-D CFD calculations included the modelling of droplets, and made use of sub-models for bubble growth and for droplet evaporation. CFD was applied initially to small scale shattered glass flasks, and then to a larger scale tank system, including the

constraints imposed as the vessel peels open. Both the detail required in calculating the initial conditions, and the results obtained, provided a greater understanding of the physical processes occurring during the important explosive expansion and turbulent growth phases, and also provided evidence to support the variation of final cloud volume as M rather than as $M^{2/3}$. The computations also demonstrated the viability of carrying out CFD simulations for this type of release.

A simple model (ACE) has been developed for the calculation of airborne concentrations following a catastrophic release of volatile material. It consists of three component sub-models:

1. explosion;
2. turbulent radial growth;
3. slumping/transport/dispersion.

Each sub-model contains a number of parameters whose values have been adjusted to be best fits to existing data. Such data are not plentiful, particularly for the phases covered by the first two stages, and the parameters and the models themselves may therefore require adjustment as further information becomes available. The model has been applied to a range of catastrophic releases which has demonstrated the sensitivity of the model to various input parameters.

Finally, it is noted that some features of the process, such as the mode of tank failure and the amount of material carried aloft by the explosion, can vary significantly even for nominally similar cases. Such variability should be borne in mind when interpreting the predictions of the model.

References

[1] D.H. Slater, Vapour clouds, Chem. Ind. (1978) 295–302.
[2] H. Lonsdale, Ammonia Tank Failure — South Africa, Vol. 17, Ammonia Plant Safety, AIChE, 1975, pp. 126–131.
[3] J. Schmidli, S. Banerjee, G. Yadigaroglu, Experiments on vapour/aerosol and pool formation on rupture of vessels containing superheated liquids, J. Loss Prev. Process Ind. 3 (1990) 104–111.
[4] S. Gilham, B.H. Mitchell, P. Woodburn, D.M. Deaves, Modelling of catastrophic flashing releases of liquid, HSE, Contract Research Report CRR 250/1999, HSE Books, 1999.
[5] N.W. Hurst, Immediate and underlying causes of vessel failures: implications for including management and organisational factors in quantified risk assessment, IChE Symposium Series No. 124, Hazards XI, New Directions in Process Safety, 1991.
[6] J. Gould, Fault tree analysis of the catastrophic failure of bulk chlorine vessels, AEA Technology Report SRD/HSE R603, AEA Consultancy Services, UK, 1993.
[7] D.A. Carter, D.M. Deaves, S.R. Porter, Reducing the risks from major toxic gas hazards, in: Loss Prevention and Safety Promotion in the Process Industries, Vol. 1, 1995.
[8] S.O. Clark, D.M. Deaves, I.G. Lines, L.C. Henson, Effects of secondary containment on source team modelling, HSE, Contract Research Report CRR 250/1999, HSE Books, 1999.
[9] US EPA Risk Management Program, Guidance for Offsite Consequence Analysis, EPA 550-B-99-009, April 1999.
[10] G. Opschoor, Methods for the Calculation of the Physical Effects of the Escape of Dangerous Material, TNO Yellow Book, 1979.
[11] Manual of Industrial Hazard Assessment Techniques, World Bank, 1985.

[12] K. Hess, W. Hoffmann, A. Stoeckel, Propagation processes after the bursting of tanks filled with liquid propane — experiments and mathematical model, in: Proceedings of the International Loss Prevention Symposium, Hague, The Netherlands, 1974, pp. 227–234.
[13] B. Hess, R. Giesbrecht, W. Leuckel, Modelling of vapour cloud dispersion and deflagration after bursting of tanks filled with liquefied gas, in: Proceedings of the 2nd International Symposium on Loss Prevention and Safety in the Process Industry, Heidelberg, 1977.
[14] D.A. Carter, Source terms, Risk analysis in the process industries, a three day workshop, IBC Technical Services Ltd., 1991.
[15] Health and Safety Executive, Canvey Island Report, HMSO, London, 1981.
[16] D.M. Johnson, M.J. Pritchard, Large scale experimental study of boiling liquid expanding vapour explosions (BLEVEs), in: Proceedings of the 14th International LNG/LPG Conference and Exhibition, Amsterdam, 4–7 December 1991.
[17] G.N. Pettitt, Characterisation of two-phase releases, Ph.D. thesis, South Bank Polytechnic, 1990.
[18] F.V. Bracco, Modelling of engine sprays, SAE Paper 850394, 1985.
[19] A.D. Gosman, S.I. Ioannides, Aspects of computer simulations of liquid-fuelled combustors, AIAA J. Energy 7 (6) (1983) 482–490.
[20] W. Rodi, Influence of buoyancy and rotation on equations for turbulent length scale, in: Proceedings of the 2nd Symposium on Turbulent Shear Flows, 1979.
[21] C.J. Wheatley, A users guide to TRAUMA — a computer code for assessing the consequences of accidental two-phase releases of NH_3 into moist air, UKAEA Report SRD/HSE R394, 1987.
[22] I.H. Dunbar, N. Hiorns, D. Mather, G. Tickle, Atomisation and Dispersion of Toxic Liquids Resulting from Accidental Pressurised Releases, Hazards XII, European Advances in Process Safety, 1984, pp. 143–153.
[23] S.R. Shield, A Model to Predict the Radiant Heat Transfer and Blast Hazards from LPG BLEVES, Vol. 89, AIChE Symposium Series, 1993.
[24] R.J. Bettis, Two phase releases following rapid vessel failure, Ph.D. thesis, South Bank Polytechnic, 1987.
[25] B.E. Launder, D.B. Spalding, The numerical computation of turbulent flow, Comp. Meth. Appl. Mech. Eng. 3 (1974) 269.
[26] P.C. Reist, Aerosol Science and Technology, 2nd Edition, McGraw-Hill, New York, 1993.
[27] D.W. Johnson, J.L. Woodward, Release: A Model with Data to Predict Aerosol Rainout in Accidental Releases, AIChE, CCPS Concept Books, 1999.
[28] S. Whitaker, Fundamental Principles of Heat Transfer, Pergamon Press, Oxford, 1977.
[29] H.C. Hardee, D.O. Lee, Expansion of clouds from pressurised liquids, Accid. Anal. Prev. 7 (1975) 91–102.